Supporting Information for

Both Zundel and Eigen Isomers Contribute to the IR Spectrum of the Gas-phase $H_9O_4^+$ cluster

Waldemar Kulig and Noam Agmon

The Fritz Haber Research Center, Institute of Chemistry,

The Hebrew University of Jerusalem, Jerusalem 91904, Israel

(Dated: December 17, 2013)

email: agmon@fh.huji.ac.il

This PDF file includes:

Supplementary Figures S1 to S32

Supplementary Tables S1 to S11

References

Other Supplementary Materials for this manuscript includes the following:

Movie S0 - trans-Z conformer (trajectory as outputted from CP2K)

Movie S1 - trans-Z conformer (structure aligned with the structure in the first frame)

Movie S2 - trans-Z · 1Ar conformer (structure aligned with the structure in the first frame)

Movie S3 - trans-Z · 2Ar conformer (structure aligned with the structure in the first frame)

Movie S4 - cis-Z conformer (structure aligned with the structure in the first frame)

Movie S5 - E conformer (structure aligned with the structure in the first frame)

Movie S6 - E · 1Ar conformer (structure aligned with the structure in the first frame)

Movie S7 - E · 2Ar conformer (structure aligned with the structure in the first frame)

Movie S8 - E · 3Ar conformer (structure aligned with the structure in the first frame)

H_3O^+

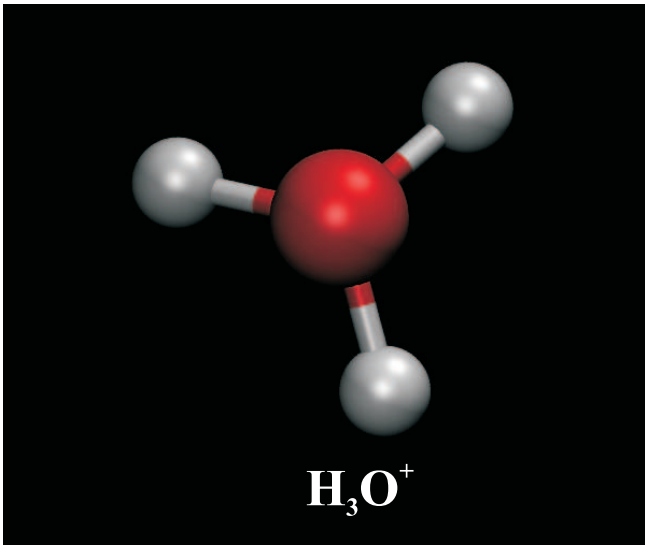

FIG. S1: Optimized structure of the H_3O^+ cation calculated at the B3LYP/aug-cc-pVTZ level of theory using Gaussian 03[2]. XYZ coordinates in Tbl. S1.

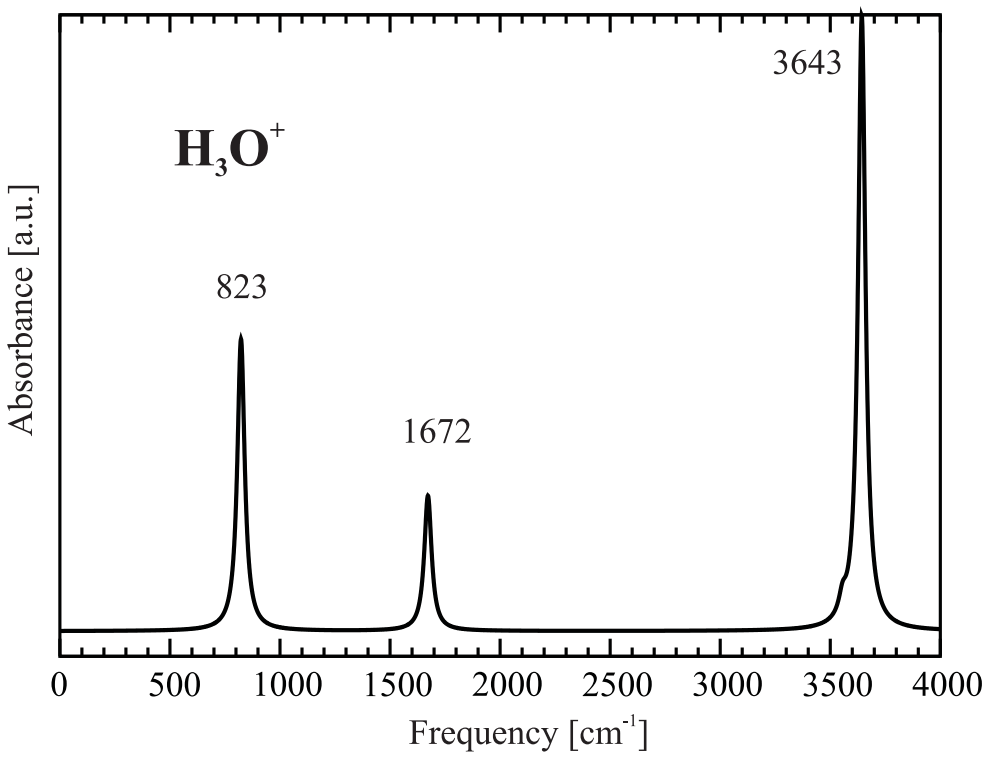

FIG. S2: Static IR spectrum of the H_3O^+ cation calculated at the B3LYP/aug-cc-pVTZ level of theory using Gaussian 03.

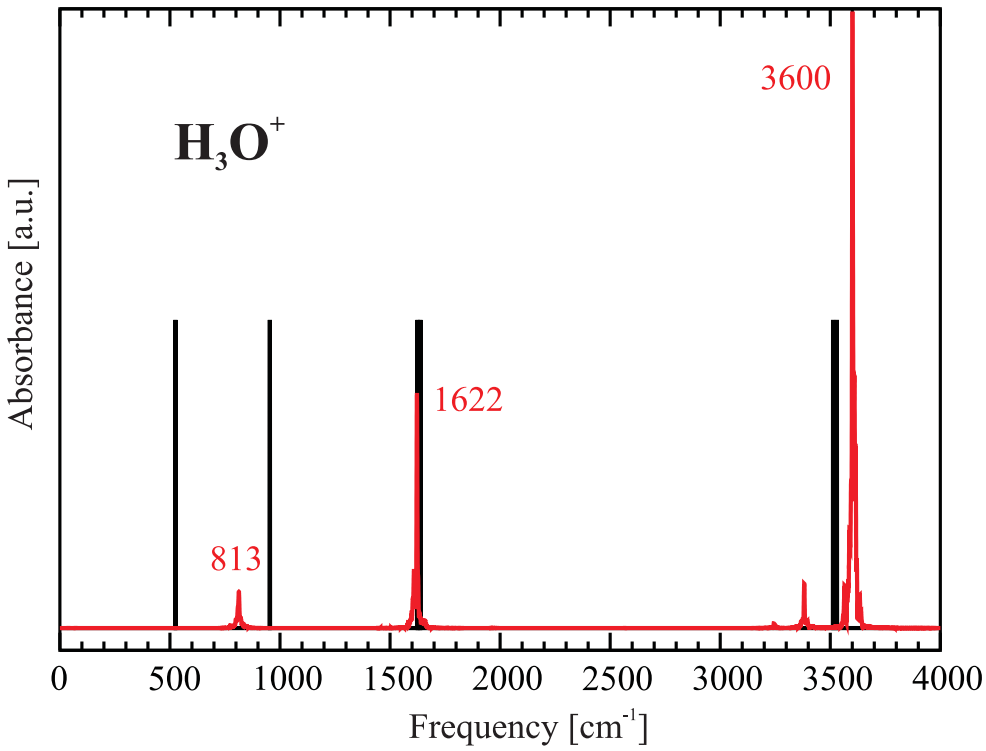

FIG. S3: Comparison between the theoretical (red) and experimental[1,3,4,7] (black) IR spectra of the H_3O^+ cation. The (dynamic) theoretical spectrum was obtained from a 10 ps CP2K AIMD simulation at 50 K as detailed above. Note the overall agreement with the static spectrum in Fig. S2, except that the peaks there are somewhat blue shifted due to the harmonic model.

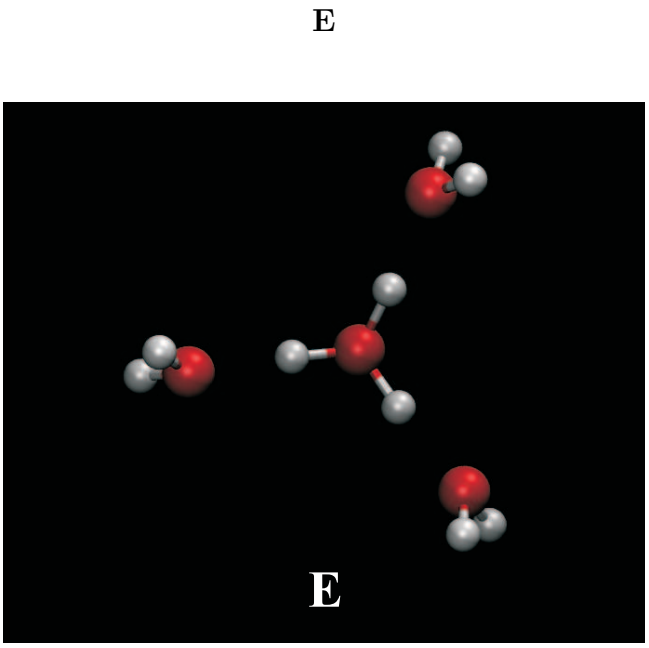

FIG. S4: The optimized structure of the E-isomer of the $H_9O_4^+$ cation calculated at the B3LYP/aug-cc-pVTZ level of theory using Gaussian 03. XYZ coordinates in Tbl. S2.

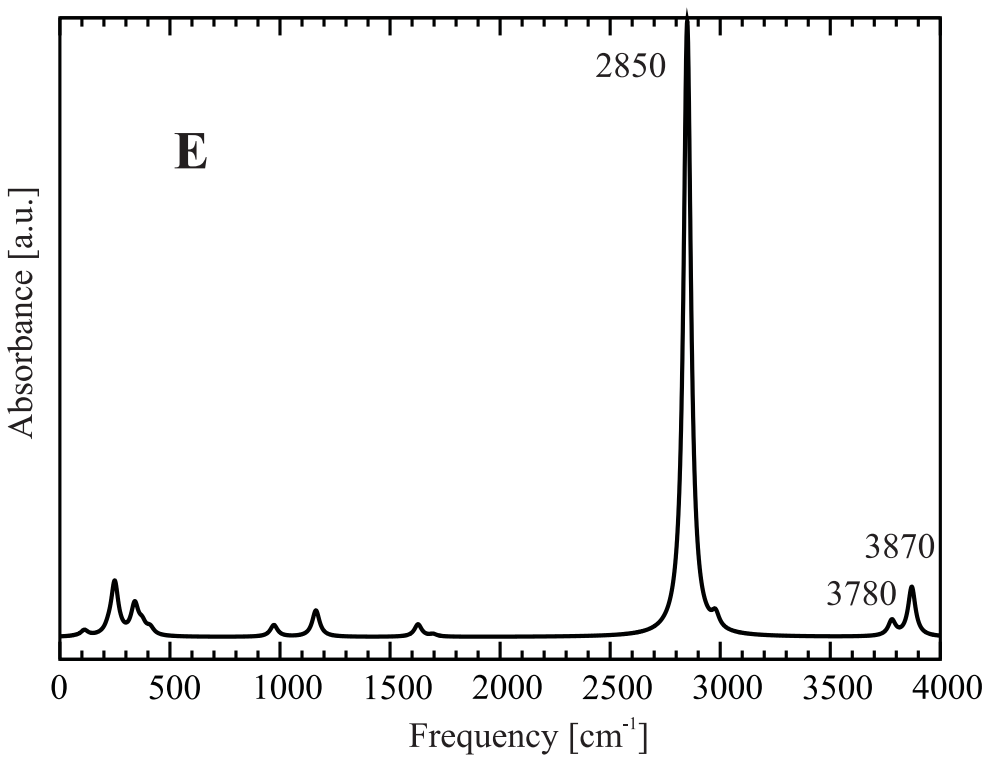

FIG. S5: Static IR spectrum of the E-isomer of $H_9O_4^+$ calculated at the B3LYP/aug-cc-pVTZ level of theory using Gaussian 03.

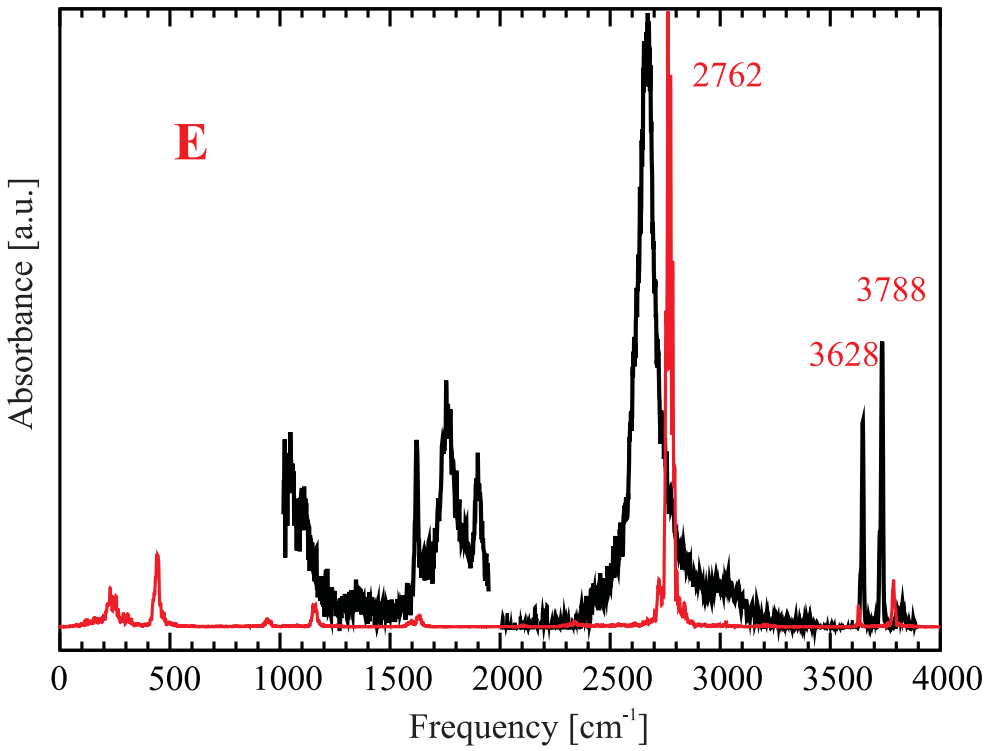

FIG. S6: Comparison between the (dynamic) theoretical (red) and experimental[5] (black) IR spectra of the E-isomer of the $H_9O_4^+$ cation. Theoretical spectrum was calculated from a 20 ps CP2K AIMD simulation at 50 K.

E · 1Ar

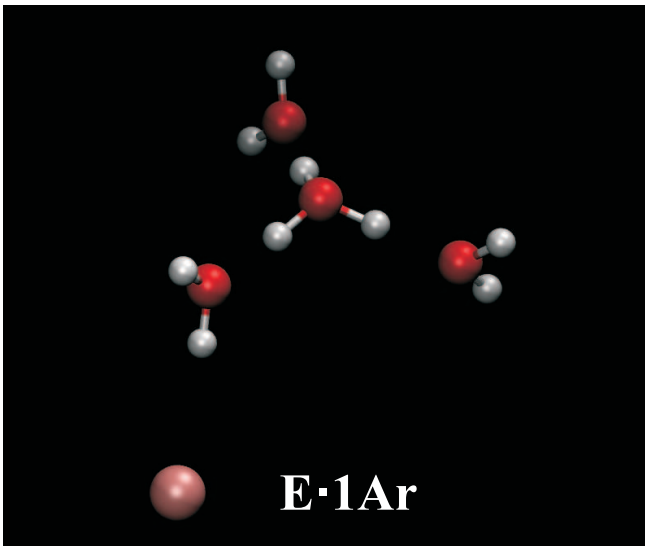

FIG. S7: The optimized structure of the E · 1Ar isomer of the $H_9O_4^+ \cdot 1Ar$ cation calculated at the B3LYP/aug-cc-pVTZ level of theory using Gaussian 03. XYZ coordinates in Tbl. S3. Argon atoms rendered in pink herein.

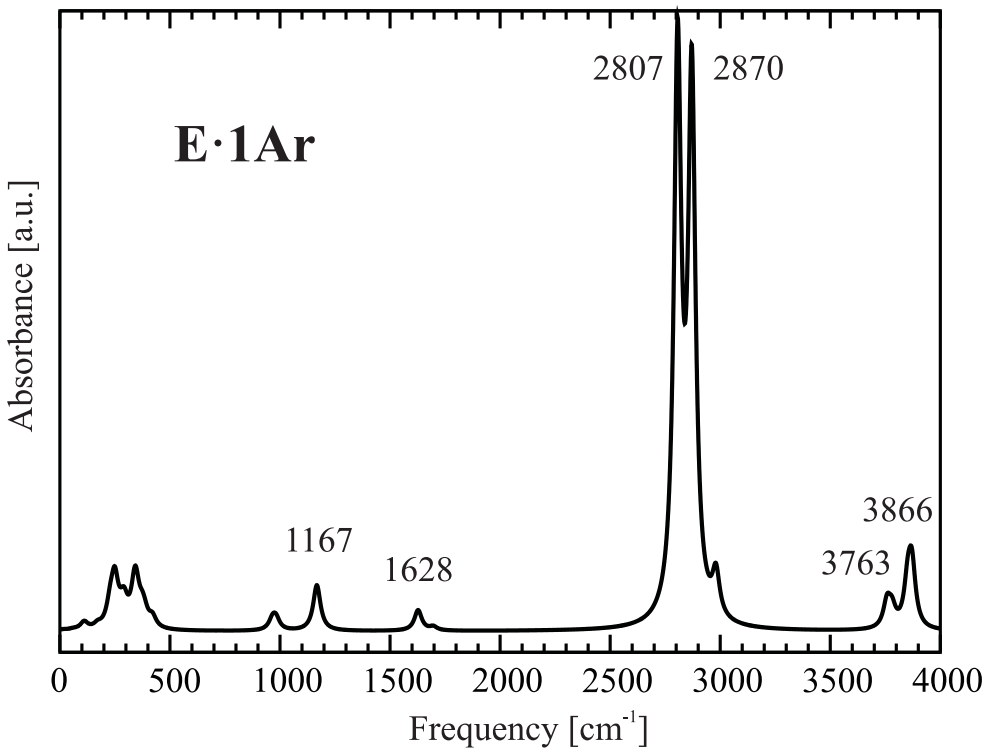

FIG. S8: Static IR spectrum of the E · 1Ar isomer of the $H_9O_4^+ \cdot 1Ar$ cation calculated at the B3LYP/aug-cc-pVTZ level of theory using Gaussian 03.

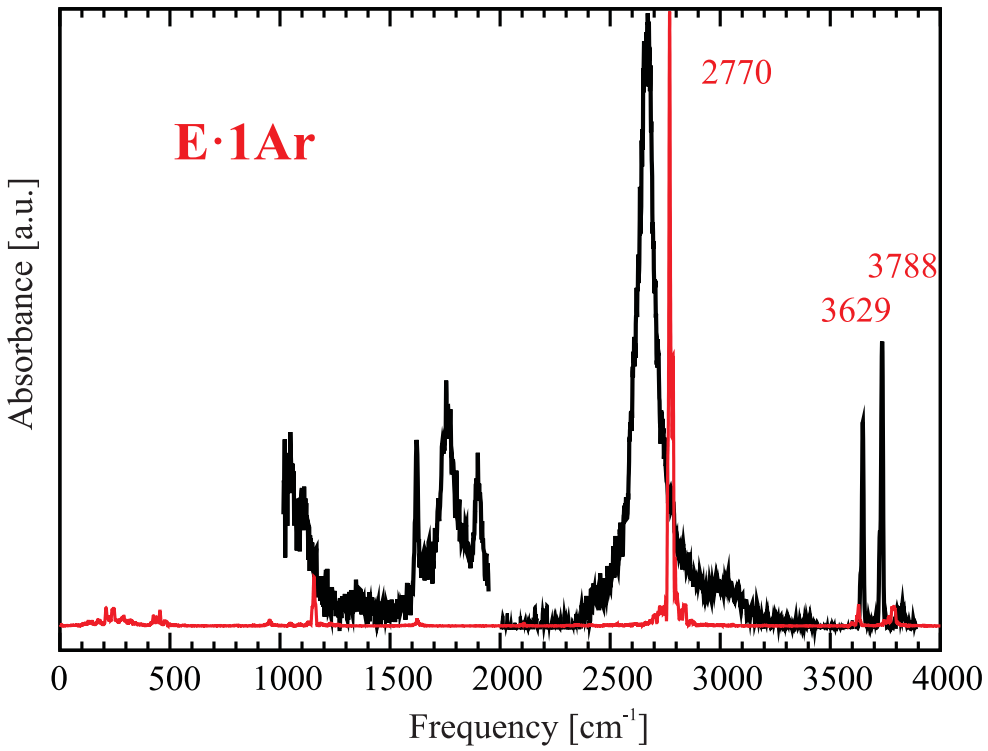

FIG. S9: Comparison between the theoretical (red) and experimental[5] (black) IR spectra of the E · 1Ar isomer of the $H_9O_4^+ \cdot 1Ar$ cation. Theoretical spectrum was obtained from a 10 ps CP2K AIMD simulation at 50 K.

E · 2Ar

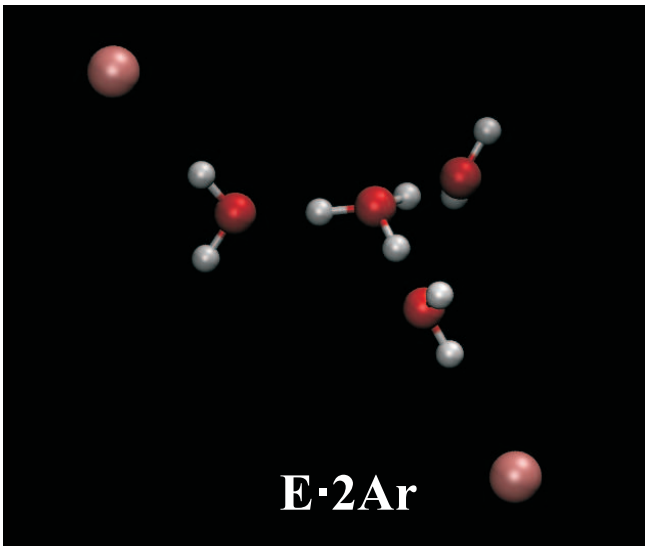

FIG. S10: The optimized structure of the E · 2Ar isomer of the $H_9O_4^+ \cdot 2Ar$ cation calculated at the B3LYP/aug-cc-pVTZ level of theory using Gaussian 03. XYZ coordinates in Tbl. S4.

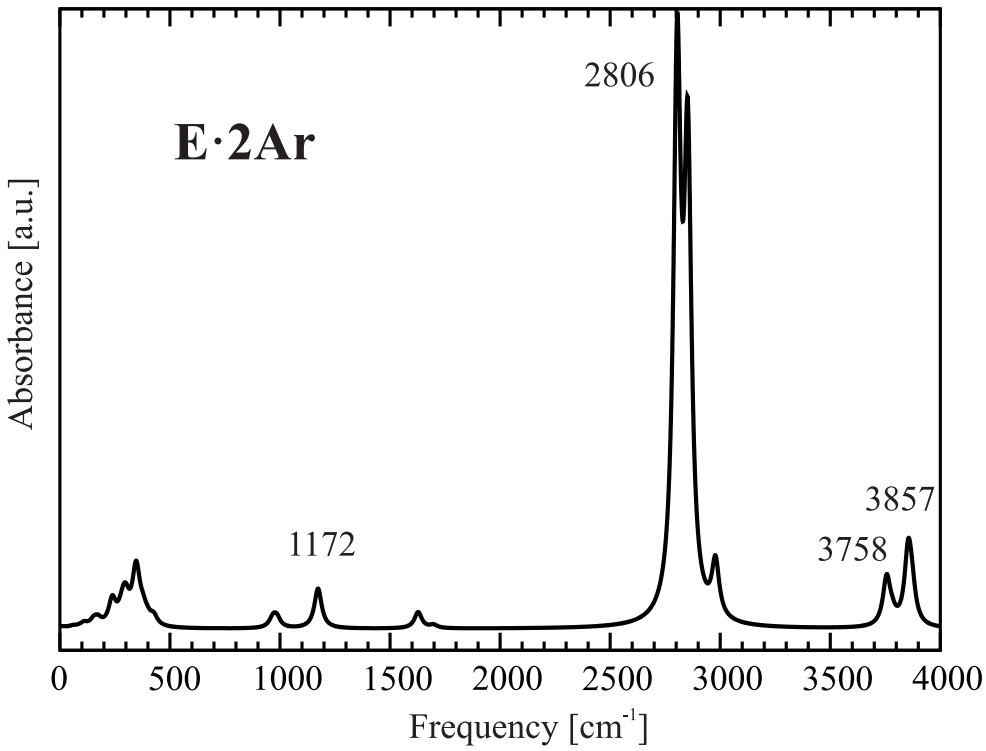

FIG. S11: Static IR spectrum of the E · 2Ar isomer of the $H_9O_4^+ \cdot 2Ar$ cation calculated at the B3LYP/aug-cc-pVTZ level of theory using Gaussian 03.

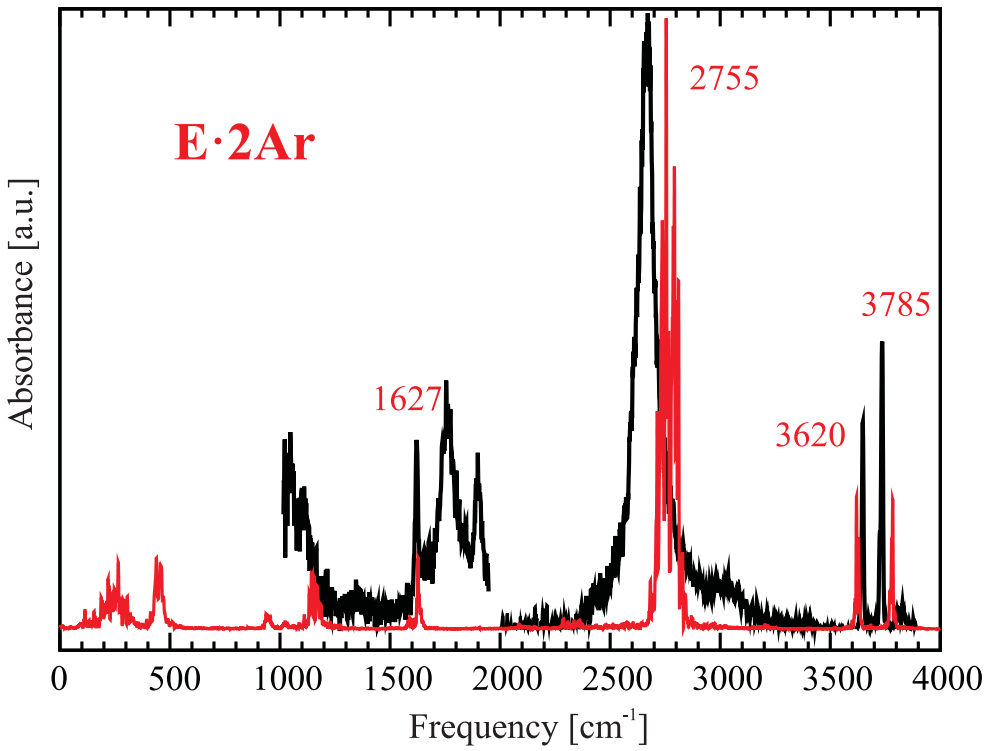

FIG. S12: Comparison between theoretical (red) and experimental[5] (black) IR spectrum of the E · 2Ar isomer of the $H_9O_4^+ \cdot 2Ar$ cation. Theoretical spectrum was obtained from a 10 ps CP2K AIMD simulation at 50 K.

E · 3Ar

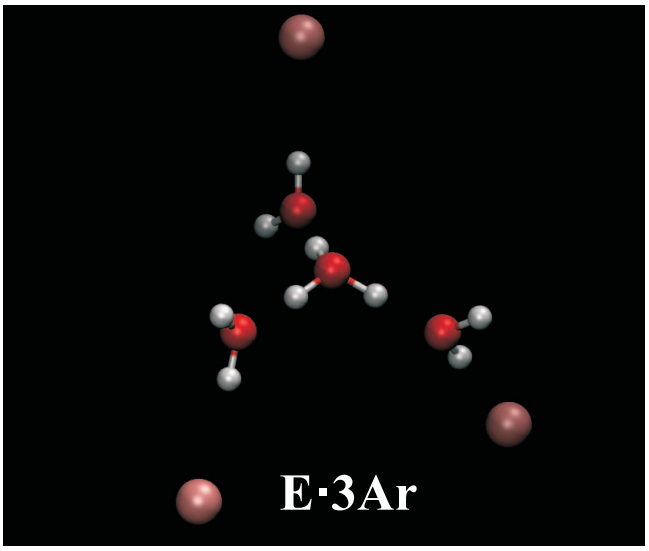

FIG. S13: The optimized structure of the E · 3Ar isomer of the $H_9O_4^+ \cdot 3Ar$ cation calculated at the B3LYP/aug-cc-pVTZ level of theory using Gaussian 03. XYZ coordinates in Tbl. S5.

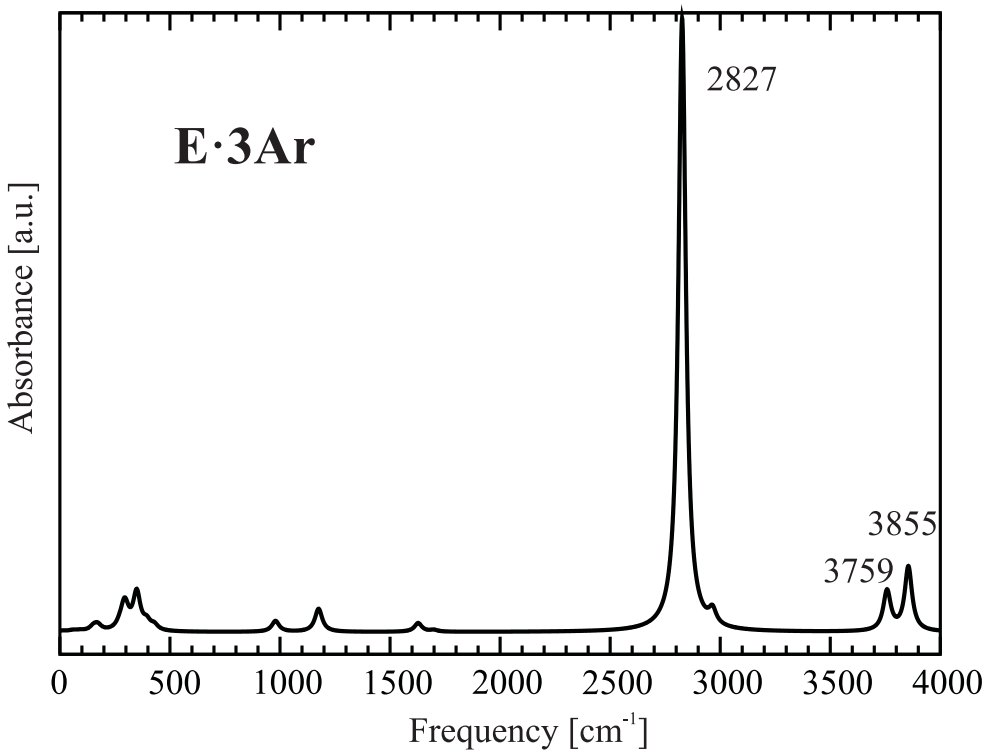

FIG. S14: Static IR spectrum of the E · 3Ar isomer of the $H_9O_4^+ \cdot 3Ar$ cation calculated at the B3LYP/aug-cc-pVTZ level of theory using Gaussian 03.

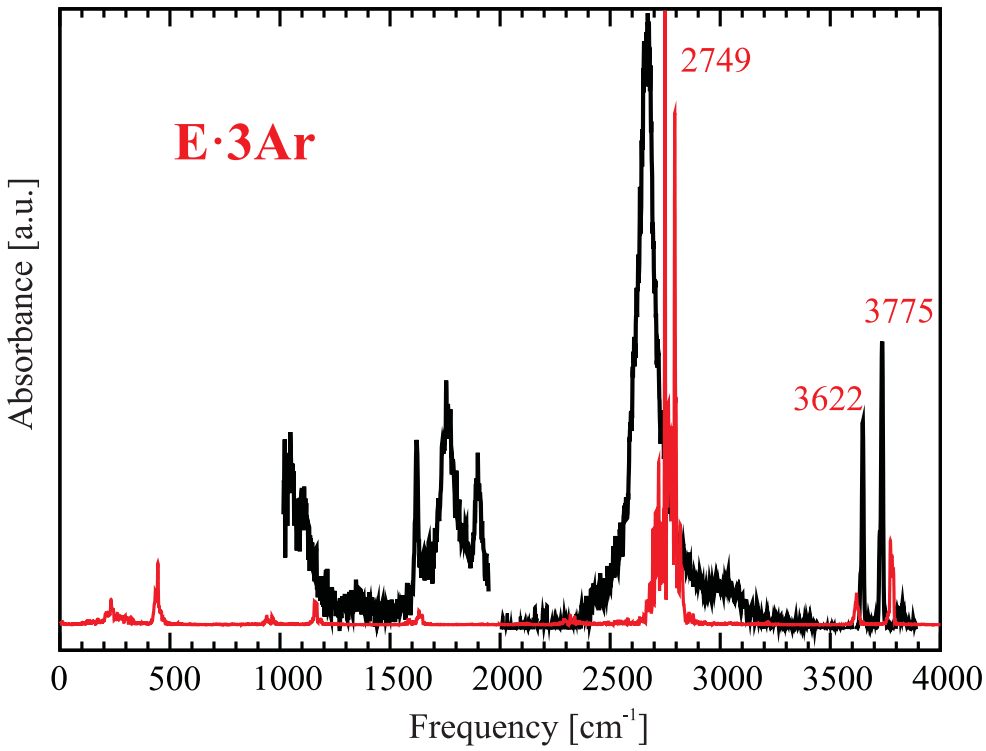

FIG. S15: Comparison between theoretical (red) and experimental[5] (black) IR spectra of the E · 3Ar isomer of the $H_9O_4^+ \cdot 3Ar$ cation. Theoretical spectrum was obtained from a 10 ps CP2K AIMD simulation at 50 K.

cis-Z

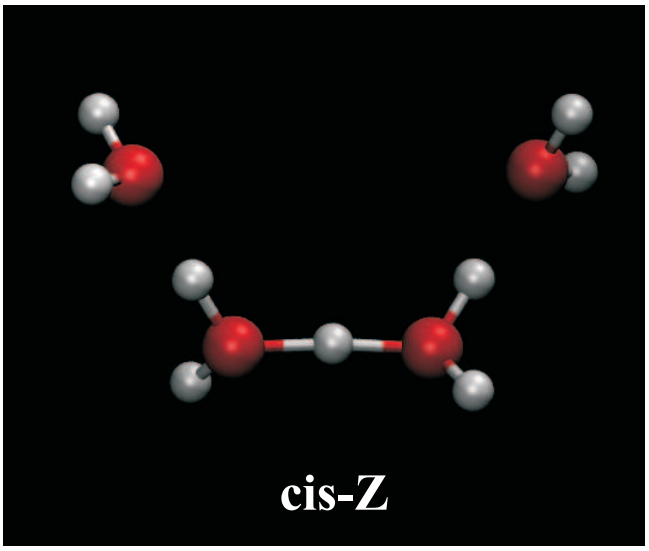

FIG. S16: The optimized structure of the cis-Z isomer of the $H_9O_4^+$ cation calculated at the B3LYP/aug-cc-pVTZ level of theory using Gaussian 03. XYZ coordinates in Tbl. S6.

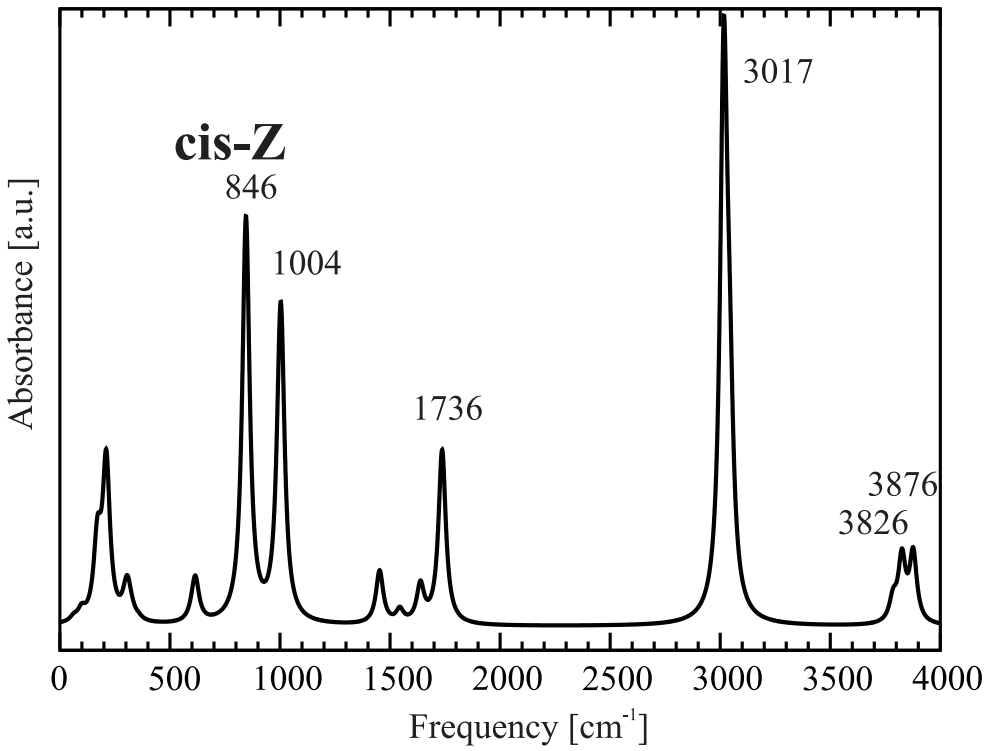

FIG. S17: Static IR spectrum of the cis-Z isomer of the $H_9O_4^+$ cation calculated at the B3LYP/aug-cc-pVTZ level of theory using Gaussian 03.

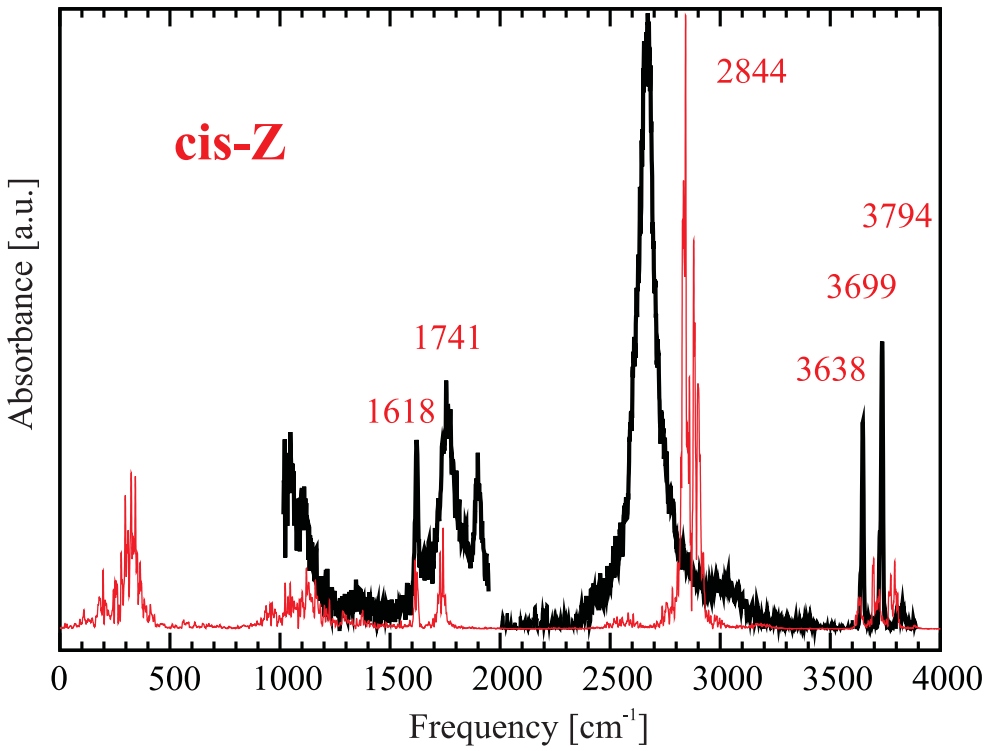

FIG. S18: Comparison between theoretical (red) and experimental[5] (black) IR spectra of the cis-Z isomer of the $H_9O_4^+$ cation. Theoretical spectrum was obtained from a 10 ps CP2K AIMD simulation at 50 K.

cis-Z · 1Ar

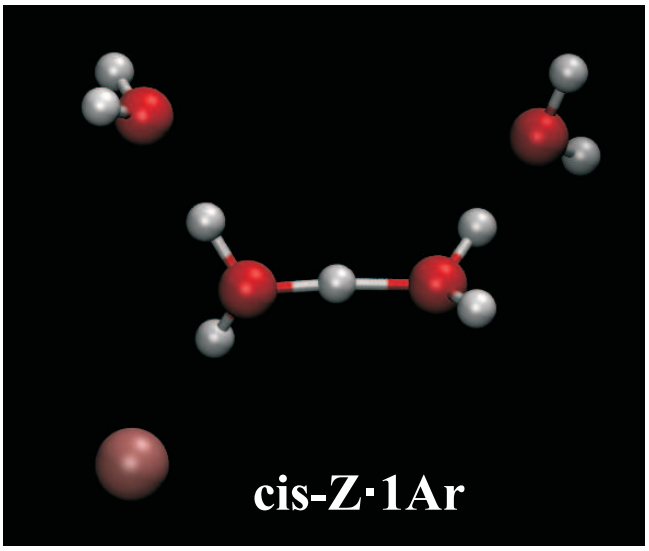

FIG. S19: The optimized structure of the cis-Z · 1Ar isomer of the $H_9O_4^+ \cdot 1Ar$ cation calculated at the B3LYP/aug-cc-pVTZ level of theory using Gaussian 03. XYZ coordinates in Tbl. S7.

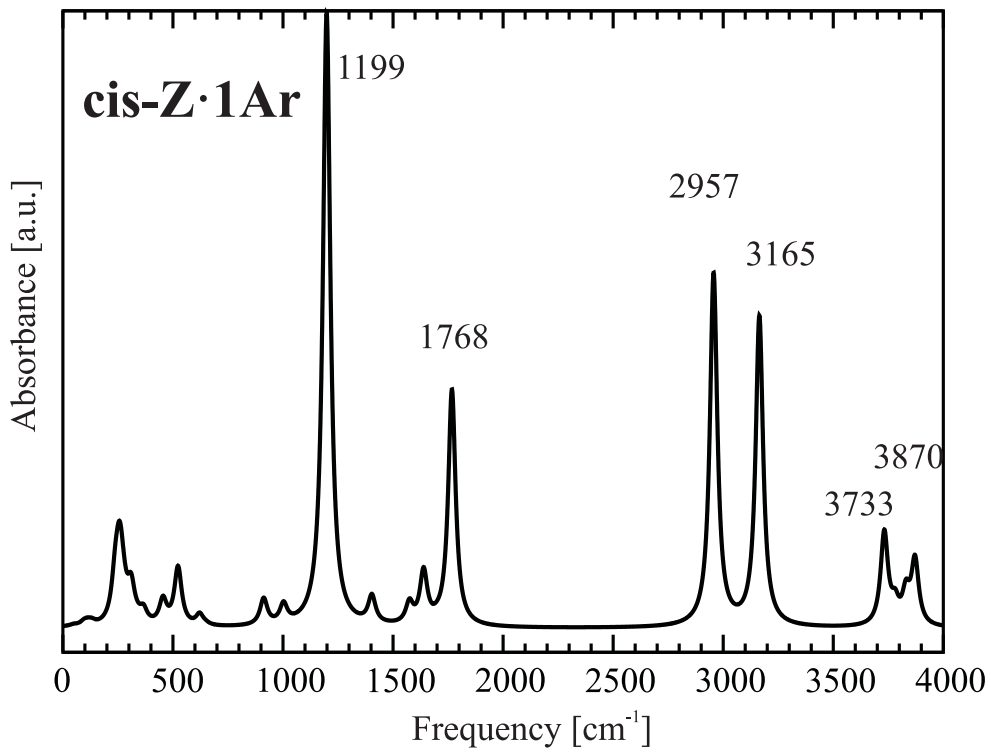

FIG. S20: Static IR spectrum of the cis-Z · 1Ar isomer of the $H_9O_4^+ \cdot 1Ar$ cation calculated at the B3LYP/aug-cc-pVTZ level of theory using Gaussian 03. There is no dynamic (CP2K) spectrum available, because this isomer converted to the trans form during CP2K equilibration.

cis-Z · 2Ar

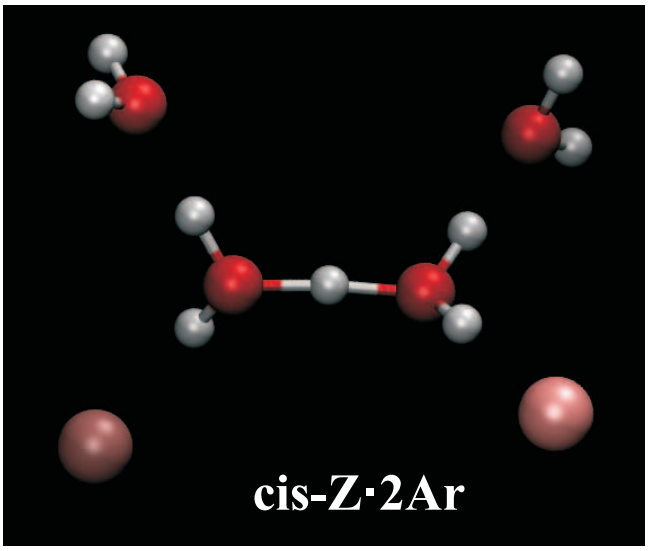

FIG. S21: The optimized structure of the cis-Z · 2Ar isomer of the $H_9O_4^+ \cdot 2Ar$ cation calculated at the B3LYP/aug-cc-pVTZ level of theory using Gaussian 03. XYZ coordinates in Tbl. S8.

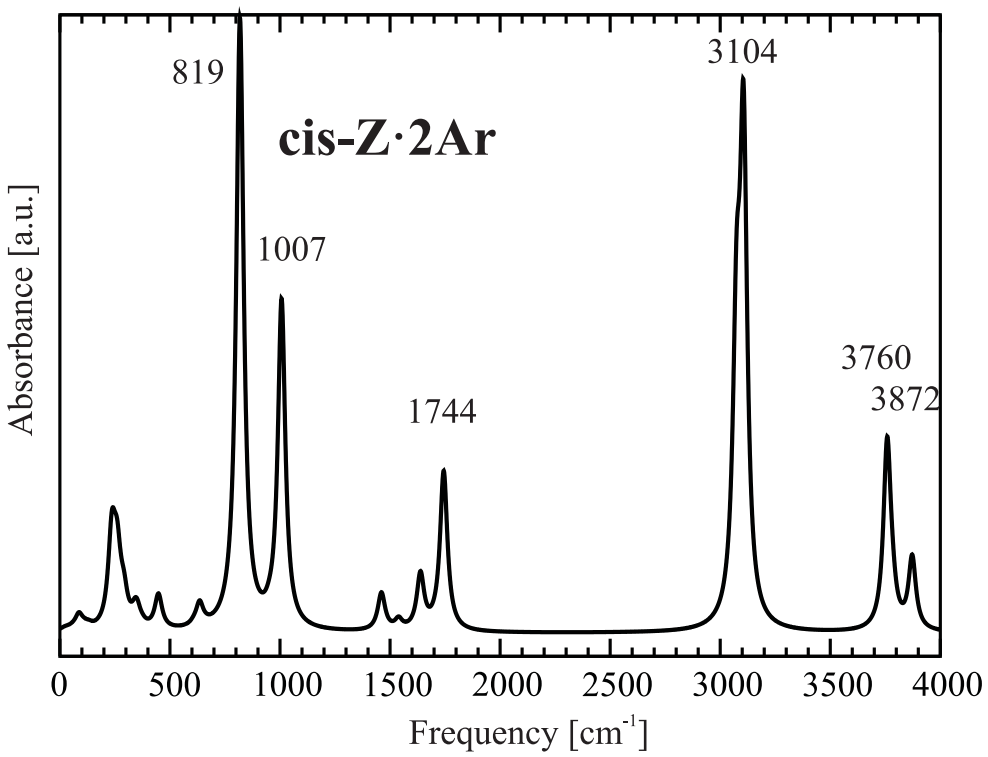

FIG. S22: Static IR spectrum of the cis-Z · 2Ar isomer of the $H_9O_4^+ \cdot 2Ar$ cation calculated at the B3LYP/aug-cc-pVTZ level of theory using Gaussian 03. There is no dynamic (CP2K) spectrum available, because this isomer converted to the trans form during CP2K equilibration.

trans-Z

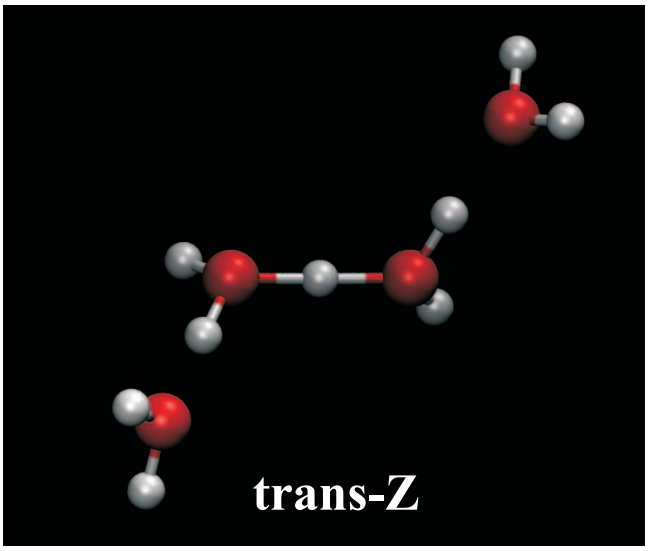

FIG. S23: The optimized structure of the trans-Z structure of the $H_9O_4^+$ cation calculated at the B3LYP/aug-cc-pVTZ level of theory using Gaussian 03. XYZ coordinates in Tbl. S9.

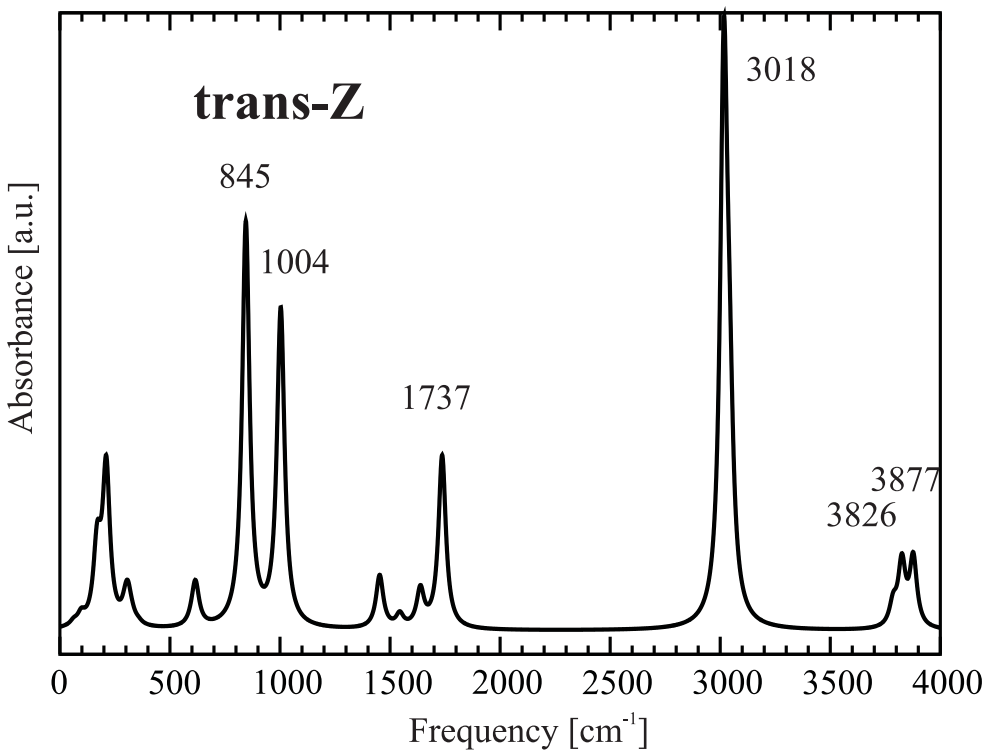

FIG. S24: Static IR spectrum of the trans-Z isomer of the $H_9O_4^+$ cation calculated at the B3LYP/aug-cc-pVTZ level of theory using Gaussian 03.

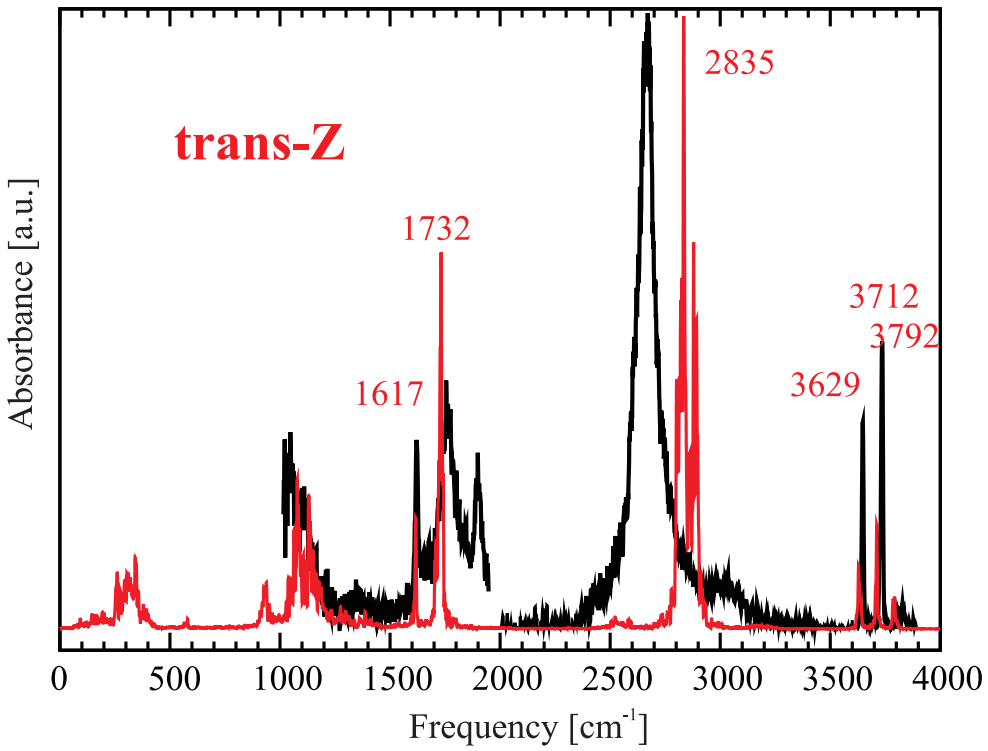

FIG. S25: Comparison between theoretical (red) and experimental[5] (black) IR spectra of the trans-Z isomer of the $H_9O_4^+$ cation. Theoretical spectrum was obtained from a 20 ps CP2K AIMD simulation at 50 K.

trans-Z · 1Ar

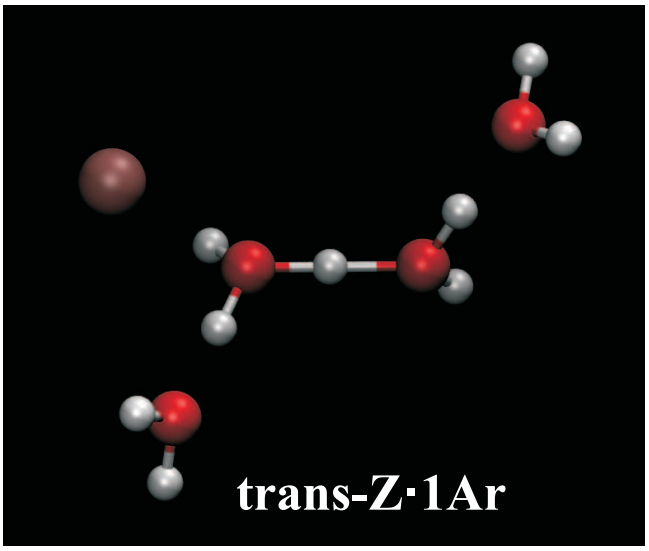

FIG. S26: The optimized structure of the trans-Z · 1Ar isomer of the $H_9O_4^+ \cdot 1Ar$ cation calculated at the B3LYP/aug-cc-pVTZ level of theory using Gaussian 03. XYZ coordinates in Tbl. S10.

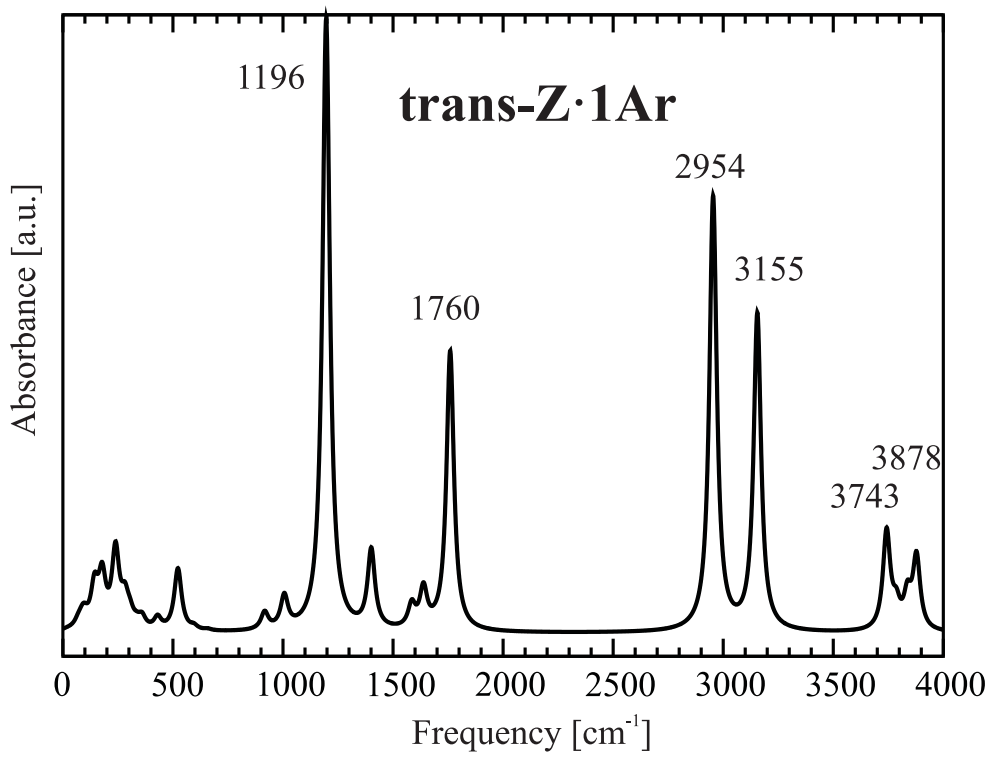

FIG. S27: Static IR spectrum of the trans-Z · 1Ar isomer of the $H_9O_4^+ \cdot 1Ar$ cation calculated at the B3LYP/aug-cc-pVTZ level of theory using Gaussian 03.

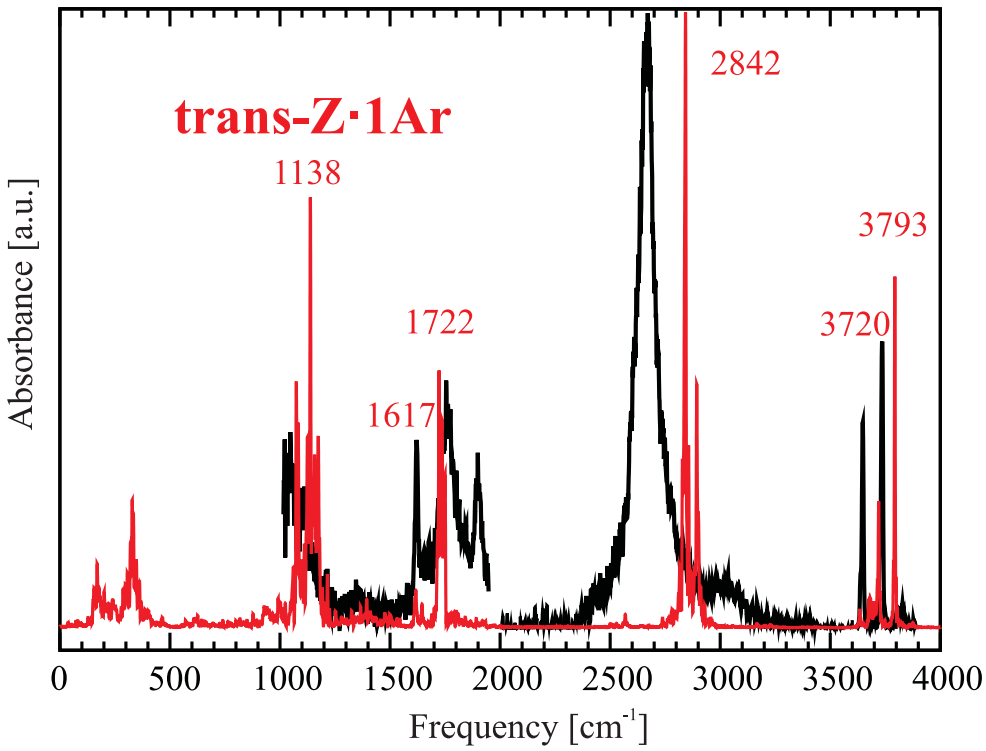

FIG. S28: Comparison between theoretical (red) and experimental[5] (black) IR spectra of the trans-Z · 1Ar isomer of the $H_9O_4^+ \cdot 1Ar$ cation. Theoretical spectrum was obtained from a 10 ps CP2K AIMD simulation at 50 K.

trans-Z · 2Ar

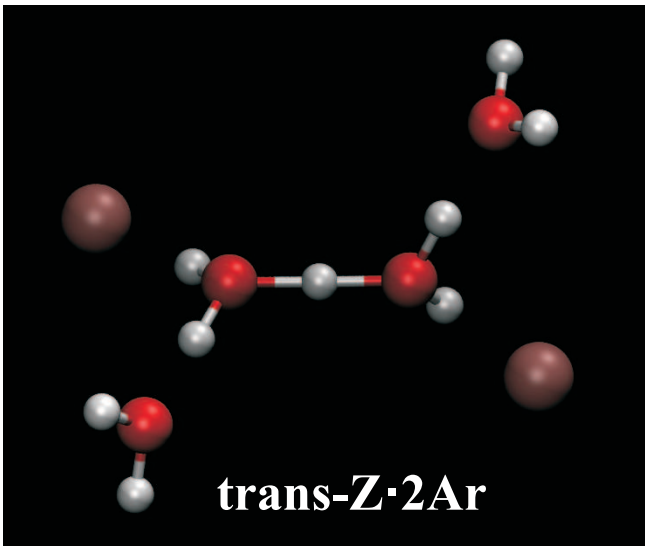

FIG. S29: The optimized structure of the trans-Z · 2Ar isomer of the $H_9O_4^+ \cdot 2Ar$ cation calculated at the B3LYP/aug-cc-pVTZ level of theory using Gaussian 03. XYZ coordinates in Tbl. S11.

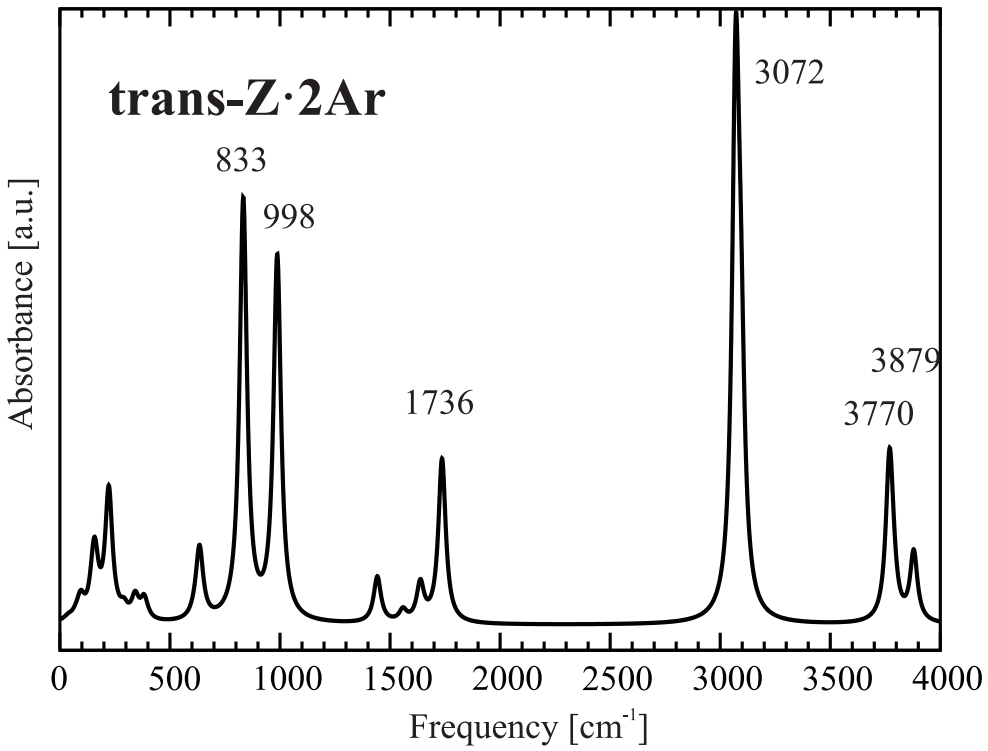

FIG. S30: Static IR spectrum of the trans-Z · 2Ar isomer of the $H_9O_4^+ \cdot 2Ar$ cation calculated at the B3LYP/aug-cc-pVTZ level of theory using Gaussian 03.

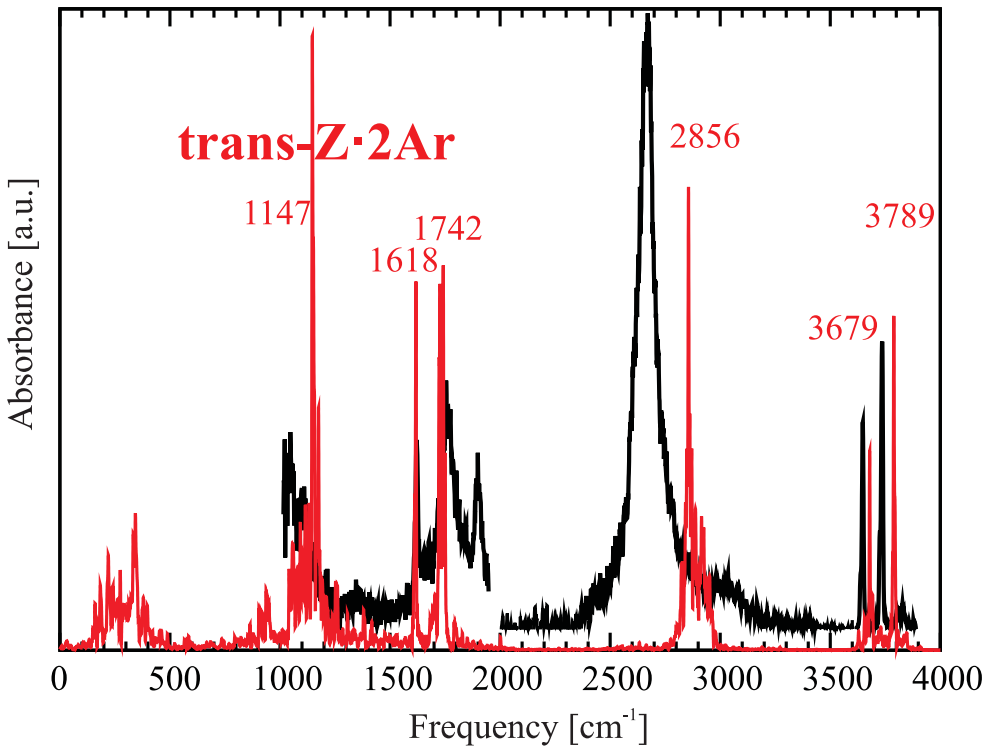

FIG. S31: Comparison between theoretical (red) and experimental[5] (black) IR spectra of the trans-Z · 2Ar isomer of the $H_9O_4^+ \cdot 2Ar$ cation. Theoretical spectrum was obtained from a 20 ps CP2K AIMD simulation at 50 K.

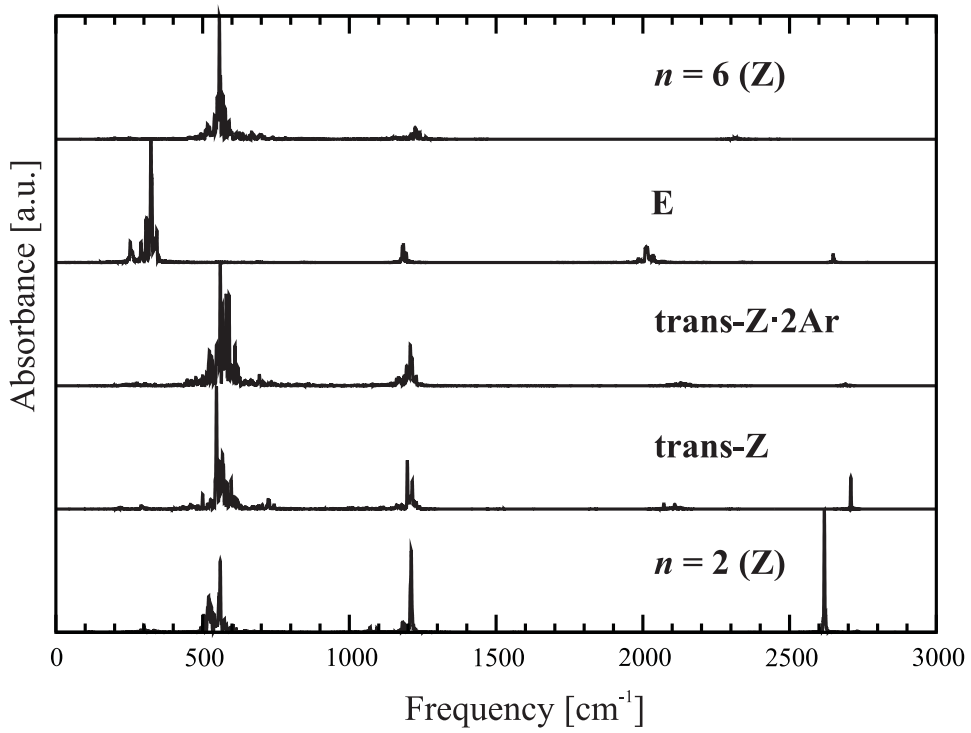

FIG. S32: Comparison between the temporal Fourier transforms of the velocity auto-correlation functions (VACF) of the O $\cdots$ O distance(s) closest to the protonated core (3 distances for an E-cation and a single one for a Z-cation). Calculated from CP2K trajectories (at 50 K) for (top to bottom): $H_{13}O_6^+$ $(n = 6)^6$, three $H_9O_4^+$ isomers from the present work (E, trans-Z $\cdot$ 2Ar and trans-Z), and $H_5O_2^+$ $(n = 2)^6$.

TABLE S1: Cartesian coordinates of a local minimum of H_3O^+ cation shown in Fig. S1, calculated at B3LYP/aug-cc-pVTZ level of theory using Gaussian 03.

13

H_3O^+

O	0.01675	-0.02900	0.01145
H	-0.01338	0.02317	0.99011
H	0.92963	0.02350	-0.34244
H	-0.48516	-0.79333	-0.34245

TABLE S2: Cartesian coordinates of the local minimum of the E-isomer of $H_9O_4^+$ shown in Fig. S4, calculated at B3LYP/aug-cc-pVTZ level of theory using Gaussian 03.

13

E conformer

O	1.00926	2.31721	0.29044
H	1.26478	2.97548	-0.36585
H	1.51922	2.49848	1.08769
O	1.5042	-1.97626	-0.01368
H	1.9213	-2.44139	-0.74785
H	1.43698	-2.60125	0.71665
O	0.02346	0.06989	-0.44705
H	0.44025	0.93596	-0.12302
H	0.57735	-0.7551	-0.24393
O	-2.47001	-0.25264	0.04812
H	-3.10955	-0.29395	-0.67203
H	-2.94906	0.02304	0.83746
H	-0.95923	-0.02636	-0.21522

TABLE S3: Cartesian coordinates of the local minimum of the E · 1Ar isomer of the $H_9O_4^+ \cdot 1Ar$ cation shown in Fig. S7, calculated at the B3LYP/aug-cc-pVTZ level of theory using Gaussian 03.

14

E · 1Ar conformer

O	1.944575	-0.816139	0.656390
O	-0.082560	0.083769	-0.604912
O	-0.313078	2.639620	-0.617314
O	-2.270066	-1.213355	-0.261495
H	2.676334	-1.214509	0.171916
H	1.961297	-1.181989	1.549750
H	-2.641541	-1.741615	-0.977150
H	-2.995903	-0.988406	0.330929
H	0.695410	-0.296693	-0.070524
H	-0.963347	-0.390722	-0.445897
H	-0.202449	3.134415	-1.437195
H	-0.118381	3.244572	0.106978
H	-0.149545	1.094120	-0.570037
Ar	2.127377	-2.126070	3.906408

TABLE S4: Cartesian coordinates of the local minimum of the E · 2Ar isomer of the $H_9O_4^+ \cdot 2Ar$ cation shown in Fig. S10, calculated at the B3LYP/aug-cc-pVTZ level of theory using Gaussian 03.

15

E · 2Ar conformer

O	1.908834	-0.836514	1.154449
O	-0.023302	-0.350284	-0.445806
Ar	1.819159	-1.191205	4.647090
O	-0.265662	2.094015	-1.148977
O	-2.229451	-1.553169	0.093462
H	2.674457	-1.336367	0.849904
H	1.859196	-0.946788	2.112282
H	-2.546773	-2.266078	-0.472422
H	-2.998487	-1.184598	0.541932
H	0.712921	-0.556431	0.223805
H	-0.911076	-0.782297	-0.223657
H	-0.095144	2.358602	-2.062209
H	-0.112356	2.867615	-0.595724
H	-0.095834	0.634356	-0.688518
Ar	0.302922	3.048819	-4.471920

TABLE S5: Cartesian coordinates of the local minimum of E · 3Ar isomer of the $H_9O_4^+ \cdot 3Ar$ cation shown in Fig. S13, calculated at the B3LYP/aug-cc-pVTZ level of theory using Gaussian 03.

16			
E · 3Ar conformer			
O	2.037630	-0.753044	0.734968
O	0.016906	0.129549	-0.563521
O	-2.003633	-1.438851	-0.636405
O	-0.531196	2.597890	-0.170647
Ar	2.089924	-2.576149	3.743079
H	2.849616	-0.980439	0.268390
H	2.024933	-1.268363	1.551178
H	-2.249390	-1.870957	-1.461998
H	-2.801301	-1.384965	-0.095327
H	0.789244	-0.249868	-0.024918
H	-0.809166	-0.460619	-0.567654
H	-0.418581	3.241702	-0.881798
H	-0.452981	3.077508	0.661102
H	-0.177855	1.106732	-0.368166
Ar	-4.917777	-1.352957	1.325448
Ar	-0.184443	4.952886	-2.745713

TABLE S6: Cartesian coordinates of the local minimum of the cis-Z isomer of the $H_9O_4^+$ cation shown in Fig. S16, calculated at the B3LYP/aug-cc-pVTZ level of theory using Gaussian 03.

13

cis-Z conformer

O	0.443267	0.606642	-0.518902
H	0.406987	1.534007	-0.256797
H	1.380727	0.251643	-0.435912
H	-0.225968	0.313785	-1.469546
O	-0.978123	0.052785	-2.370000
H	-0.618448	-0.110584	-3.294638
H	-1.673025	-0.581924	-2.159728
O	-0.036652	-0.247105	-4.766864
H	-0.341931	0.326918	-5.478612
H	0.259107	-1.067079	-5.177492
O	2.811314	-0.416526	-0.274612
H	3.640705	-0.045774	-0.595739
H	3.026089	-0.954697	0.495815

TABLE S7: Cartesian coordinates of the local minimum of the cis-Z · 1Ar isomer of the $H_9O_4^+ \cdot 1Ar$ cation shown in Fig. S19, calculated at the B3LYP/aug-cc-pVTZ level of theory using Gaussian 03.

14

cis-Z · 1Ar conformer

O	0.434194	0.740127	-0.467287
O	-0.882534	0.103093	-2.382280
O	2.838907	-0.196568	-0.002584
O	0.253084	-0.213328	-4.670414
H	0.341394	1.654523	-0.178485
H	1.366497	0.424795	-0.300857
H	-0.221599	0.388646	-1.505493
H	-0.439885	-0.070142	-3.274198
H	-1.540725	-0.577308	-2.177182
H	-0.017298	0.328659	-5.420441
H	0.625730	-1.026104	-5.029611
H	3.676825	0.206199	-0.255170
H	3.010325	-0.712207	0.793385
Ar	-3.244645	-2.240239	-1.654432

TABLE S8: Cartesian coordinates of the local minimum of the cis-Z · 2Ar isomer of the $H_9O_4^+ \cdot 2Ar$ cation shown in Fig. S21, calculated at the B3LYP/aug-cc-pVTZ level of theory using Gaussian 03.

15

cis-Z · 2Ar conformer

O	0.425327	0.639208	-0.442023
O	-0.848609	0.008611	-2.374359
O	2.845947	-0.253364	-0.084391
O	0.292053	-0.261186	-4.698891
H	0.322830	1.565185	-0.183306
H	1.373717	0.340781	-0.314711
H	-0.170910	0.309962	-1.432357
H	-0.414136	-0.144003	-3.265023
H	-1.520225	-0.665699	-2.203491
H	0.013728	0.291500	-5.437863
H	0.658219	-1.067677	-5.077959
H	3.667891	0.166692	-0.360356
H	3.052836	-0.783632	0.693435
Ar	-3.340520	-2.287505	-1.729592
Ar	-0.057801	3.901849	0.564314

TABLE S9: Cartesian coordinates of the local minimum of the trans-Z isomer of the $H_9O_4^+$ cation shown in Fig. S23, calculated at the B3LYP/aug-cc-pVTZ level of theory using Gaussian 03.

13
trans-Z conformer
O -4.081647 -4.764178 4.650822
H -4.932538 -5.213430 4.608411
H -3.968065 -4.454787 5.556175
O -2.604109 -3.904112 2.710684
H -3.209906 -4.240202 3.440879
H -3.040406 -3.212034 2.201155
O 1.323712 -5.103701 1.602484
H 1.937771 -5.715853 2.022577
H 1.844559 -4.517671 1.043080
O -1.229779 -5.516815 1.586752
H -1.942254 -4.700040 2.104707
H -0.239561 -5.340190 1.556091
H -1.529696 -5.904238 0.756775

TABLE S10: Cartesian coordinates of the local minimum of the trans-Z · 1Ar isomer of the $H_9O_4^+ \cdot 1Ar$ cation shown in Fig. S26, calculated at the B3LYP/aug-cc-pVTZ level of theory using Gaussian 03.

14

trans-Z · 1Ar conformer

O	-4.013834	-4.843458	4.688090
O	-2.586644	-3.917307	2.762534
O	-1.212194	-5.522632	1.604401
O	1.381359	-5.178515	1.637772
H	-4.827766	-5.357093	4.652088
H	-3.899927	-4.547780	5.597984
H	-3.179022	-4.288858	3.492850
H	-3.055617	-3.256878	2.232697
H	1.979420	-5.809942	2.051934
H	1.919935	-4.606027	1.081388
H	-1.965763	-4.663260	2.175956
H	-0.223962	-5.379062	1.581219
H	-1.500677	-5.936612	0.784325
Ar	-4.161379	-1.486580	0.958389

TABLE S11: Cartesian coordinates of the local minimum of the trans-Z · 2Ar isomer of the $H_9O_4^+ \cdot 2Ar$ cation shown in Fig. S29, calculated at the B3LYP/aug-cc-pVTZ level of theory using Gaussian 03.

15

trans-Z · 2Ar conformer

O	-3.999257	-4.804498	4.766656
O	-2.565818	-3.924712	2.786008
O	-1.185095	-5.531939	1.661557
O	1.378822	-5.120388	1.738426
H	-4.822950	-5.302986	4.747011
H	-3.885644	-4.480306	5.666643
H	-3.151001	-4.267713	3.525054
H	-3.030905	-3.252379	2.270907
H	1.986785	-5.743259	2.151222
H	1.911020	-4.500656	1.228481
H	-1.898668	-4.718790	2.180222
H	-0.197529	-5.355270	1.654393
H	-1.470314	-5.892854	0.811794
Ar	-4.153815	-1.436361	0.988125
Ar	-2.227052	-6.928895	-1.323709

[1] M. H. Begemann, C. S. Gudeman, J. Pfaff, and R. J. Saykally. Detection of the hydronium ion (H_3O^+) by high-resolution infrared spectroscopy. *Phys. Rev. Lett.*, 51:554–557, 1983.

[2] M. J. Frisch, G. W. Trucks, H. B. Schlegel, G. E. Scuseria, M. A. Rob, J. R. Cheeseman, J. A. Montgomery Jr., T. Vreven, K. N. Kudin, J. C. Burant, J. M. Millam, S. S. Iyengar, J. Tomasi, V. Barone, B. Mennucci, M. Cossi, G. Scalmani, N. Rega, G. A. Petersson, H. Nakatsuji, M. Hada, M. Ehara, K. Toyota, R. Fukuda, J. Hasegawa, M. Ishida, T. Nakajima, Y. Honda, O. Kitao, H. Nakai, M. Klene, X. Li, J. E. Knox, H. P. Hratchian, J. B. Cross, V. Bakken, C. Adamo, J. Jaramillo, R. Gomperts, R. E. Stratmann, O. Yazyev, A. J. Austin, R. Cammi, C. Pomelli, J. W. Ochterski, P. Y. Ayala, K. Morokuma, G. A. Voth, P. Salvador, J. J. Dannenberg, V. G. Zakrzewski, S. Dapprich, A. D. Daniels, M. C. Strain, O. Farkas, D. K. Malick, A. D. Rabuck, K. Raghavachari, J. B. Foresman, J. V. Ortiz, Q. Cui, A. G. Baboul, S. Clifford, J. Cioslowski, B. B. Stefanov, G. Liu, A. Liashenko, P. Piskorz, I. Komaromi, R. L. Martin, D. J. Fox, T. Keith, M. A. Al-Laham, C. Y. Peng, A. Nanayakkaraand M. Challacombe, P. M. W. Gill, B. Johnson, W. Chen, M. W. Wong, C. Gonzalez, and J. A. Pople. *Gaussian 03*. Gaussian Inc., Wallingford, CT, 2003.

[3] Martin Gruebele, Mark Polak, and Richard J. Saykally. A study of the structure and dynamics of the hydronium ion by high resolution infrared laser spectroscopy. ii. the ν_4 perpendicular bending mode of H_3O^+. *J. Chem. Phys.*, 87:3347–3351, 1987.

[4] Nathan N. Haese and Takeshi Oka. Observation of the ν_2 ($1^- \leftarrow 0^+$) inversion mode band in H_3O^+ by high resolution infrared spectroscopy. *J. Chem. Phys.*, 80(1):572–573, 1984.

[5] Jeffrey M. Headrick, Eric G. Diken, Richard S. Walters, Nathan I. Hammer, Richard A. Christie, Jun Cui, Evgeniy M. Myshakin, Michael A. Duncan, Mark A. Johnson, and Kenneth D. Jordan. Spectral signatures of hydrated proton vibrations in water clusters. *Science*, 308:1765–1769, 2005.

[6] Waldemar Kulig and Noam Agmon. A 'clusters-in-liquid' method for calculating infrared spectra identifies the proton transfer mode in acidic aqueous solution. *Nature Chem.*, 5:29–35, 2013.

[7] Di-Jia Liu, Nathan N. Haese, and Takeshi Oka. Infrared spectrum of the ν_2 vibration-inversion band of H_3O^+. *J. Chem. Phys.*, 82:5368–5372, 1985.